

2023

## The Effect of Process Parameters on the Properties of Elastic Melt Blown Nonwovens: Air pressure and DCD

Li Change

*College of Textiles and Clothing, Qingdao University, Qingdao, China*

Yanfen Zhou

*College of Textiles and Clothing, Qingdao University, Qingdao, China*

Stephen Jerrams

*Technological University Dublin, [stephen.jerrams@tudublin.ie](mailto:stephen.jerrams@tudublin.ie)*

*See next page for additional authors*

Follow this and additional works at: <https://arrow.tudublin.ie/cerart>

 Part of the [Chemical Engineering Commons](#)

### Recommended Citation

Change, Li; Zhou, Yanfen; Jerrams, Stephen; Ma, Jianwei; and Chen, Shaojuan, "The Effect of Process Parameters on the Properties of Elastic Melt Blown Nonwovens: Air pressure and DCD" (2023). *Articles*. 32.

<https://arrow.tudublin.ie/cerart/32>

This Article is brought to you for free and open access by the Centre for Elastomer Research at ARROW@TU Dublin. It has been accepted for inclusion in Articles by an authorized administrator of ARROW@TU Dublin. For more information, please contact [arrow.admin@tudublin.ie](mailto:arrow.admin@tudublin.ie), [aisling.coyne@tudublin.ie](mailto:aisling.coyne@tudublin.ie), [gerard.connolly@tudublin.ie](mailto:gerard.connolly@tudublin.ie), [vera.kilshaw@tudublin.ie](mailto:vera.kilshaw@tudublin.ie).



This work is licensed under a [Creative Commons Attribution-Share Alike 4.0 International License](#).


Funder: Key Technology Research and Development Program of Shandong, Grant/Award Number: 2018GGX108003

---

**Authors**

Li Change, Yanfen Zhou, Stephen Jerrams, Jianwei Ma, and Shaojuan Chen

# The effect of process parameters on the properties of elastic melt blown nonwovens: Air pressure and DCD

Li Chang<sup>1</sup> | Yanfen Zhou<sup>1</sup> | Kun Dai<sup>1</sup> | Liang Jiang<sup>1</sup>  | Stephen Jerrams<sup>2</sup> | Jianwei Ma<sup>1</sup> | Shaojuan Chen<sup>1</sup>

<sup>1</sup>College of Textiles and Clothing, Qingdao University, Qingdao, China

<sup>2</sup>Centre for Elastomer Research, Focas Research Institute, Dublin Institute of Technology, Dublin, Ireland

## Correspondence

Shaojuan Chen and Liang Jiang, College of Textiles and Clothing, Qingdao University, Qingdao, 266071, China.  
Email: [qdchshj@qdu.edu.cn](mailto:qdchshj@qdu.edu.cn) and [liang.jiang@qdu.edu.cn](mailto:liang.jiang@qdu.edu.cn)

## Funding information

Key Technology Research and Development Program of Shandong, Grant/Award Number: 2018GGX108003

## Abstract

An elastic masterbatch and elastic melt blown nonwovens are prepared based successively on styrene-ethylene/butylene-styrene (SEBS) and polypropylene (PP) blend. The phase separation morphology, rheological properties and crystal structure of the elastic masterbatch are investigated. The results show that a compatible and stable structure is obtained in molten SEBS and PP blend with excellent mobility in the temperature range of 210–230°C. The crystallization of PP slows down resulting in a finer structure due to the restriction of the SEBS network structure with rarely change of crystalline structure. The relationship between process parameters and properties of the elastic nonwoven is also studied in detail. Air pressure and die to collector distance (DCD) have discernible effects on fiber diameter and bonding between fibers, further influencing the performances of nonwovens including porosity, tensile strength and elastic recovery. Elastic recovery is shown to be significantly more affected by DCD than by air pressure.

## KEYWORDS

air pressure, DCD, elastic recovery, melt blown nonwovens

## 1 | INTRODUCTION

Melt blown nonwovens have been widely used in numerous applications including personal hygiene care, medical protection, bandaging for wounds,<sup>1</sup> filtration medium,<sup>2</sup> oil absorption.<sup>3</sup> They are suitable for such applications because excellent barrier properties arise from having micro/nano fibers and porous structures, high surface areas, and economic viability highlighted by Wentz.<sup>4</sup> Particularly with the outbreak of COVID-19, melt blown nonwovens and their functional products have played an important role in limiting the spread of the virus and protecting human health.<sup>5,6</sup>

The materials normally used for melt blowing primarily include polypropylene (PP), polyester (PET) and polylactic acid (PLA).<sup>7,8</sup> However, these materials have the

disadvantages of small elongations and low elasticity, which restrict their further applications such as garments, support clothing and personal hygiene products where more freedom of body movement is required.<sup>9,10</sup> To improve the toughness and elasticity of melt blown nonwoven, commercial thermoplastic elastomers, including polyurethane (PU), styrene-ethylene/butylene-styrene (SEBS) and polyolefin (POE), have been investigated when used directly<sup>11–15</sup> or blended for melt blowing.<sup>16–18</sup> Among these candidates, SEBS with saturated molecular chains, shows promise because of its excellent properties of weather resistance, UV resistance, resistance to aging and working temperature range when compared with PU and POE.<sup>13,19,20</sup> It has been used for obtaining elastic nonwoven fabrics by electrospinning,<sup>21,22</sup> whereas, it has some unfavorable characteristics for melt blowing, such

as high melt elasticity, high melt viscosity and stickiness.<sup>9,23</sup> SEBS was usually blended with PP as a modifier or compatibilizer to enhance the impact strength of PP<sup>24,25</sup> or its compatibility with other polymers.<sup>26</sup> In some studies, blending with PP was also found to improve the flowability of SEBS.<sup>27</sup> However, few studies on the spinnability of SEBS and PP blends.

The elasticity of SEBS derives from the micro-phase separation between polystyrene (PS) blocks as physical cross-links, and EB blocks as flexible regions.<sup>28</sup> If blended with PP the flowability of SEBS will improve, but a high content of the PP component inevitably increases the crystallinity of blends, which breaks the physical crosslinking structure of SEBS, leading to a reduction of elasticity and resilience. In previous work,<sup>29</sup> the influence of PP content on the elasticity of SEBS/PP blends was studied. It was found that when PP content was above 10 wt%, although the melt viscosity and tensile strength improved, the elastic recovery decreased to below 70%. Consequently, SEBS mixed with 10 wt% PP was selected as the raw material, termed SPB in this text, to manufacture elastic melt blown nonwovens in the research described here.

In reality, not only the properties of the raw materials affect the structure and characteristics of melt blown nonwovens, but also the processing parameters during melt blowing have a strong influence. These include the polymer throughput, melting and stretching temperatures, air pressure, die to collector distance (DCD), and the rotational speed of collector. There are complex inter-relationships between these parameters<sup>4,8</sup> that have significant influences on the structure and properties of the nonwovens. The polymer throughput and the rotational speed of collector are usually adjusted according to the output and the basis weight of product. The melting and stretching temperatures are determined by the melt flow properties of polymers, and there is a narrow processing window in actual production. However, the air pressure and DCD greatly influence the forming of fibers from molten polymer drops, further resulting in a variation of morphology and properties of nonwovens.

There have been numerous studies on the relationship between process parameters and the properties of PP melt blown nonwovens,<sup>30–32</sup> but studies on the effect of

DCD and air pressure into the elasticity of melt blown nonwovens are rare. In this work, the crystallinity and rheological properties were initially analyzed as well as the phase separation phenomenon of the blend. Thereafter, elastic melt-blown nonwovens were obtained by adjusting the parameters of air pressure and DCD. The relationship between the parameters and the properties of nonwovens, including fiber diameter, porosity, the tensile strength, and the elastic recovery performance, were further investigated.

## 2 | EXPERIMENTAL

### 2.1 | Materials

The elastic masterbatch SPB was prepared in the laboratory by a co-rotating twin-screw extruder based on SEBS and PP at a mass ratio of 90:10. PP HP461Y was supplied by PolyMirae, Korea. SEBS MD1648 (PS/EB = 20:80 wt%) was purchased from Kraton Polymers, USA. The melt blending temperature was set at 190°C and the screw speed was 30 rpm.

### 2.2 | Manufacture of the elastic melt-blown nonwovens

The elastic nonwovens were manufactured using a lab-scale melt blown machine (die capillary diameter = 300 μm and spinneret width = 350 mm) customized by Sunhoo Automation Equipment Co., Ltd. (China, SH-RBJ). The temperatures of the extruder zone were set in the range of 160–220°C. As listed in Table 1, the DCD and air pressure were adjusted to investigate the effects on nonwoven structure and properties.

### 2.3 | Characterizations

Using a VEGA3SBH scanning electron microscope (SEM, TESCAN, Czech Republic), the cryo-fractured surfaces of masterbatches and the slices of nonwoven fibers were

**TABLE 1** Processing parameters of the process to produce elastic melt-blown nonwovens

Sample code	DCD (cm)	Air pressure (kPa)	Basis weight (g m <sup>-2</sup> )	Thickness of the nonwoven (mm)
1	20	47	94.16	0.64
2	20	58	80.44	0.53
3	20	70	99.16	0.63
4	25	70	79.92	0.53
5	30	70	101.36	0.75

observed after being coated with gold. The fiber diameters were statistically analyzed utilizing the Image Pro Plus 6.0 software based on 100 fibers for each sample.

The viscoelastic properties of samples were investigated by using a dynamic rheometer (MCR302, ANTON PAAR, Austria) under an N<sub>2</sub> atmosphere. The parallel plate was 50 mm diameter and the gap was 1 mm. The frequency sweep was in the range of 6.28–628 rad s<sup>-1</sup> under a strain amplitude of 5% at temperatures of 170, 190, 210, 230, and 250°C, respectively.

The melting and crystallization behaviors of the masterbatches were determined by a differential scanning calorimeter (DSC 3+, METTLER TOLEDO, Switzerland). The temperatures ranged from 30 to 250°C at a scanning rate of 10°C min<sup>-1</sup> conducted under an N<sub>2</sub> atmosphere.

The X-ray diffraction pattern and lattice parameters of the samples was obtained by employing an X-ray diffractometer (XRD, SmartLab SE, Rigaku, Japan) using Cu K $\alpha$  radiation with a wavelength of 0.15406 nm. The measurements were conducted in a reflection mode with a scan range of 5–70°, a scanning speed of 10° min<sup>-1</sup>, and a step width was 0.01°.

The crystal morphology was observed by polarized optical microscopy (POM, Axio scope A1 POL, Carl Zeiss, Germany). The samples were molten at 220°C for 5 min, then pressed with a glass slide to form films. Isothermal crystallization was continued for 30 min at temperatures of 90 and 50°C, respectively for PP and SPB.

The porosity of the nonwoven fabric was calculated using Equation (1),<sup>33</sup>

$$P = 1 - \frac{\rho_w}{\rho_f} = 1 - \frac{m}{\delta \times \rho_f}, \quad (1)$$

where  $P$  is porosity,  $\rho_w$  is the density of the nonwoven fabric,  $\rho_f$  is the density of the polymer (0.91 g cm<sup>-3</sup> for SPB),  $m$  is the basis weight of the nonwoven fabric, and  $\delta$  is the thickness of the nonwoven fabric.

The tensile properties of nonwovens were tested according to ASTM D 5035 on an electronic tensile testing machine (5965, INSTRON, USA). Samples with a gauge length of 50 mm and width of 25 mm were stretched at a speed of 100 mm min<sup>-1</sup>.

The elastic recovery rate was evaluated by measuring the length change after the stretch and relaxation process and using Equation (2). The samples were stretched to 100% elongation and held for 1 min, then returned. The length when the load force was returned to zero was considered as the final length after recovery. Both the rate of stretch and recovery were at 100 mm min<sup>-1</sup>.

$$r = \frac{l_1 - l_2}{l_1 - l_0}, \quad (2)$$

where  $r$  is the elastic recovery rate,  $l_0$  and  $l_1$  are the lengths before and after stretching (50 mm and 100 mm respectively for this test),  $l_2$  is the final length after recovery.

## 3 | RESULTS AND DISCUSSION

### 3.1 | Morphology observations

For two-phase blends, the distribution between the phases will affect the properties of the material and have an impact on the processing. The cross-sections of SEBS, PP and SPB masterbatch are shown in Figure 1. It can be observed that the SEBS had a rough morphology exhibiting many ripples, while the fracture of the PP had a smooth surface. Ripples can be observed on the fracture surface of the SPB but the surface is much smoother than that of SEBS as shown in Figure 1c, d, indicating that the rigidity of SEBS had been enhanced with the addition of PP.

Although the SPB had an obvious ‘sea-island’ structure where the PP did not agglomerate in the rich phase of SEBS, there was no obvious boundary between the two phases (shown in Figure 1e), which indicated a semi-compatibility between PP and SEBS due to the similar molecular structure of PP and EB segment of the SEBS. The distribution of PP in the SEBS was uniform, which is beneficial for the mobility and spinnability of the elastic masterbatch.

### 3.2 | Crystallization analysis

To eliminate the effect of thermal history during processing, the second melting curve and crystallization curves of the specimens were used as shown in Figure 2a, b. There is no melting peak and crystalline peak in the curves of SEBS. The peak around 79°C in the melting curve is assigned to the glass transition ( $T_g$ ) of the PS region.<sup>20</sup> The results demonstrate that the SEBS used in this work was an amorphous copolymer, while the PP used here is a typical semi-crystalline polymer with melting peaks at 155°C and 163°C corresponding to the incomplete and perfect crystallizations respectively. The melting peak of SPB appears at around 160°C with a narrower melting range than the PP. The crystalline temperature ( $T_c$ ) of SPB (88°C) is lower than that of PP (111°C). The increase in the degree of undercooling (the difference between the melting temperature and the crystallization temperature) of SBP (72.05°C) compared to PP (51.44°C) indicated a slower crystallization and finer crystalline structure (as observed by POM). The reason for this may be that the entanglement of molecular

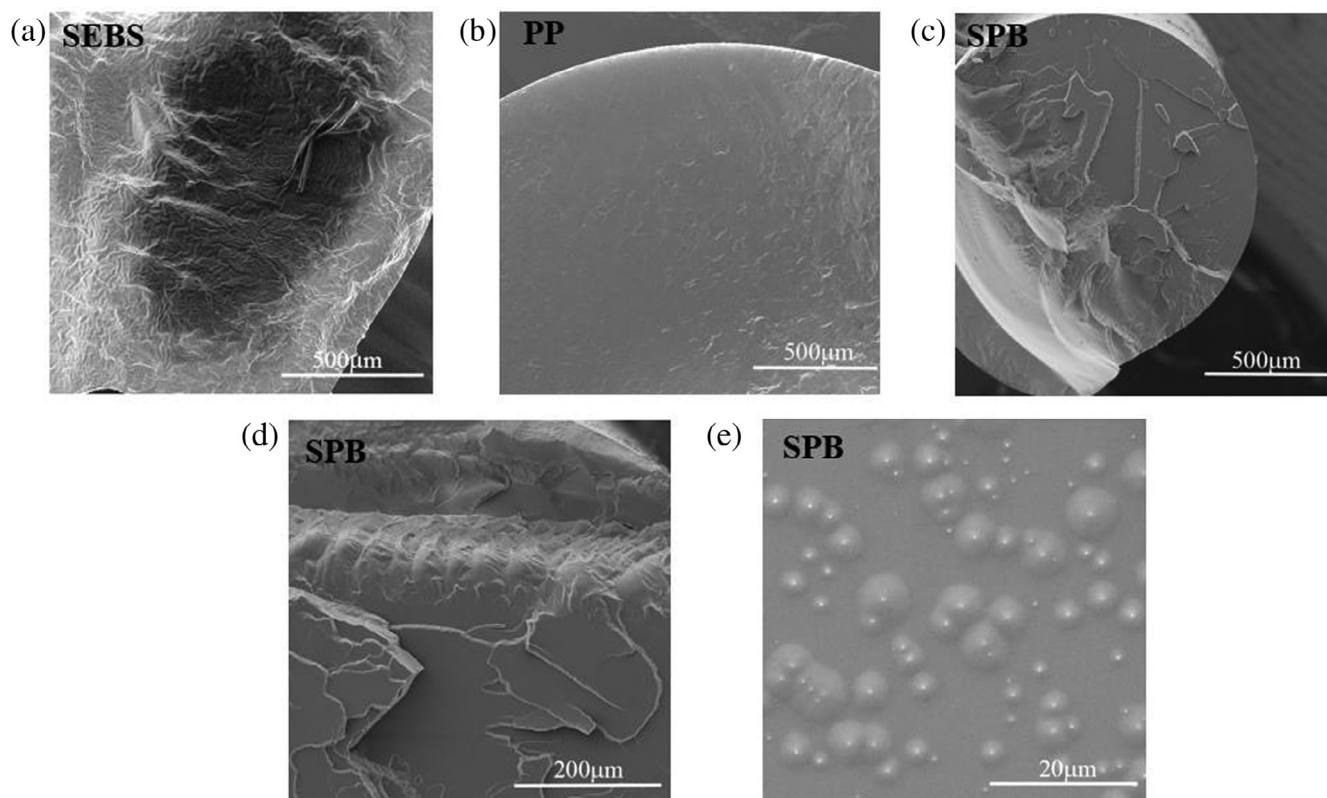


FIGURE 1 SEM images of the cross-section of: (a) SEBS, (b) PP, (c) SPB; (d) and (e) are for SPB at higher magnifications

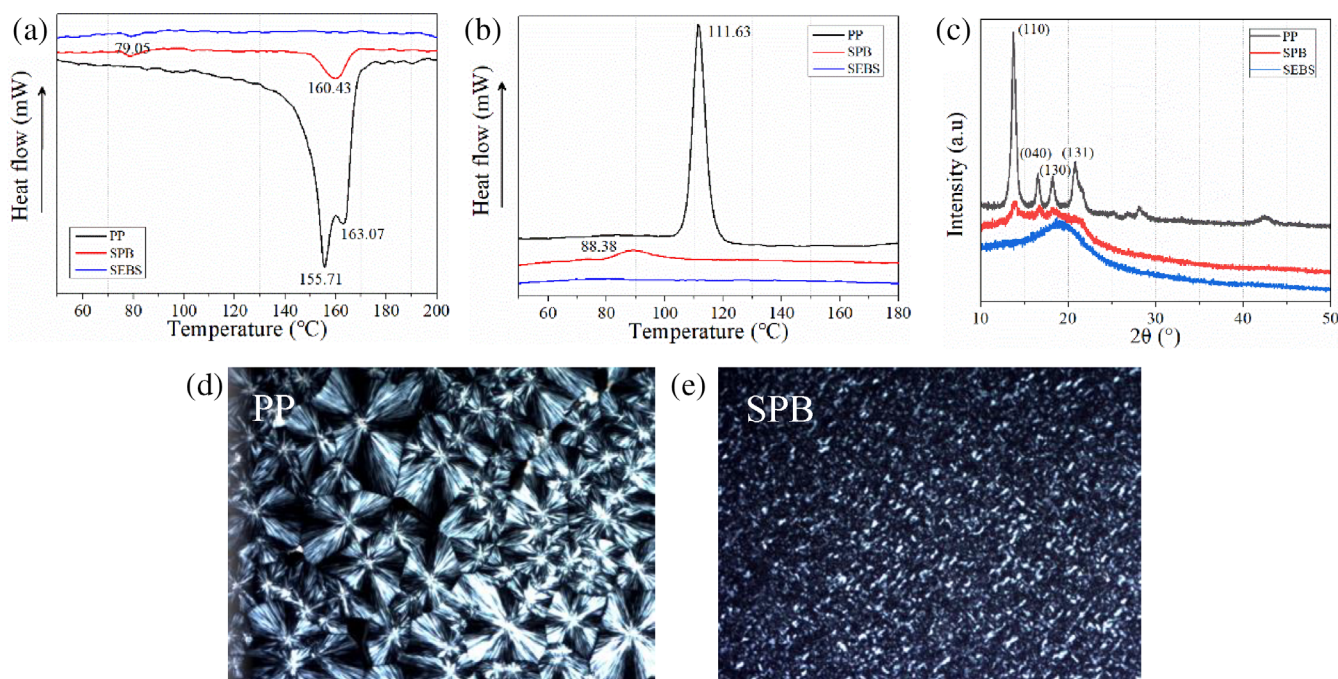


FIGURE 2 DSC curves and crystallization of SEBS, PP and SPB: (a) second melting curves, (b) calorimetric crystallization curves, (c) XRD curves, (d) and (e) POM photographs [Color figure can be viewed at [wileyonlinelibrary.com](https://onlinelibrary.wiley.com/terms-and-conditions)]

chains between SEBS and PP restricted the nucleation velocity as well as the diffusion and orderly accumulation of PP chains to crystal nuclei.

The XRD spectrum of specimens are shown in Figure 2c. The crystal size ( $L_{hkl}$ ) and interplanar spacing ( $d$ ) were calculated by Debye–Scherrer Equation (3) and

**TABLE 2** The crystalline parameters of PP and SPB

Lattice plane	Crystal size ( $L_{hkl}$ , nm)		Interplanar spacing ( $d$ , Å)	
	PP	SPB	PP	SPB
(110)	15.677	7.526	6.431	6.394
(040)	19.162	7.934	5.345	5.287
(130)	15.027	5.073	4.883	4.858
(131)	7.358	4.443	4.263	4.198

Bragg Equation (5),<sup>34</sup> and the results are listed in Table 2. Compared with pure PP, there was no new diffraction peaks appearing for SPB, and the position of the peaks were similar to that of PP. The interplanar spacing was almost unchanged, but the crystal size was decreased indicating that SEBS hindered the growth of PP crystals while having no effect on the crystalline structure.

$$L_{hkl} = \frac{k\lambda}{\beta_0 \cos \theta}, \quad (3)$$

$$\beta_0 = \sqrt{\beta^2 - b_0^2}, \quad (4)$$

$$d = \frac{\lambda}{2 \sin \theta}, \quad (5)$$

where  $k$  is the instrument constant (0.9),  $\lambda$  is the radiation wavelength of 0.15406 nm,  $\beta_0$  is the half-width of the reflection corrected for the instrumental broadening according to Equation (4),  $\beta$  is the half-width of various diffraction peaks,  $b_0$  is the instrumental broadening factor (0.15°),  $\theta$  is the Bragg angle.

Since SEBS is an amorphous and isotropic block polymer, it does not exhibit any polarization phenomenon. Polarized optical microscope photographs of specimens of PP and SPB are shown in Figure 2d, e. PP spherulites grew with black cross and distinct interfaces between crystals. For SPB there was clearly a great number of crystalline masses observed and the interfaces between crystals were blurred. This may be because the amorphous EB blocks when dispersed in PP was difficult to be separated from the crystal growth surfaces due to high compatibility between EB and PP, which hindered the growth of spherulites.<sup>35</sup>

### 3.3 | Rheological property analysis

The rheological property of the material is crucial for melt blowing process and is greatly affected by temperature and shear force, as a result, it is necessary to investigate the rheological property of the material to obtain the suitable processing conditions.

The rheological properties of SEBS, PP and SPB are illustrated in Figure 3. It can be seen from Figure 3a that the complex viscosity ( $\eta^*$ ) of SPB decreased with increases in temperature. When the temperature reached 250°C, the  $\eta^*$  became insensitive to the angular frequency, meaning increased screw speed at higher temperatures cannot effectively decrease the viscosity of the melt. Therefore, the rheological properties were characterized below 250°C.

The  $\eta^*$  and storage modulus ( $G'$ ) of SEBS, PP and SPB versus angular frequency ( $\omega$ ) at 210°C are depicted in Figure 3b. The  $\eta^*$  of SEBS and SPB decreased with increasing frequency in a high angular frequency range, where the materials perform in accordance with typical non-Newtonian flows, while PP at this temperature showed Newtonian behavior and the viscosity of PP rarely changed with frequency increases. The non-Newtonian index ( $n$ ) of PP approached unity. The  $G'$  of SPB is between that of pure SEBS and pure PP at high angular frequency, the curve of SPB is close to that of SEBS but separated from that of PP, which is due to the smaller volume fraction of PP in SPB samples.<sup>36–38</sup> However, in the low frequency range, it became higher than that of SEBS and PP. This may be attributed to the phase separation induced by low frequency shear,<sup>39</sup> where the dispersed PP molecules oriented along the forces, obstructed the movement of SEBS molecules, resulting in a high storage modulus.

Cole-Cole plots of imaginary dynamic viscosity ( $\eta''$ ) versus the real dynamic viscosity ( $\eta'$ ) can reflect the phase separation phenomenon. When the polymer has a linear molecular structure, the Cole-Cole curve is semi-circular. However, when there are multiple phase domains or phase separations in the polymer or blend, the curve will have upturned tails or two semi-circles.<sup>40</sup> Figure 3c illustrates the Cole-Cole plots of SPB at different temperatures. The curve has an obvious tail at the low angular frequency region at 170°C, for high values of  $\eta'$ , that may have arisen from micro-separation between the two phases of SEBS and the shape relaxation of PP. As temperature increased, the degree of upturning of the tail became weaker, and when it reached 210°C and 230°C, the curves presented a semicircular shape, which demonstrated that SEBS was well integrated and had superior compatibility with PP in this temperature range. As the temperature continued to rise to 250°C, the curve

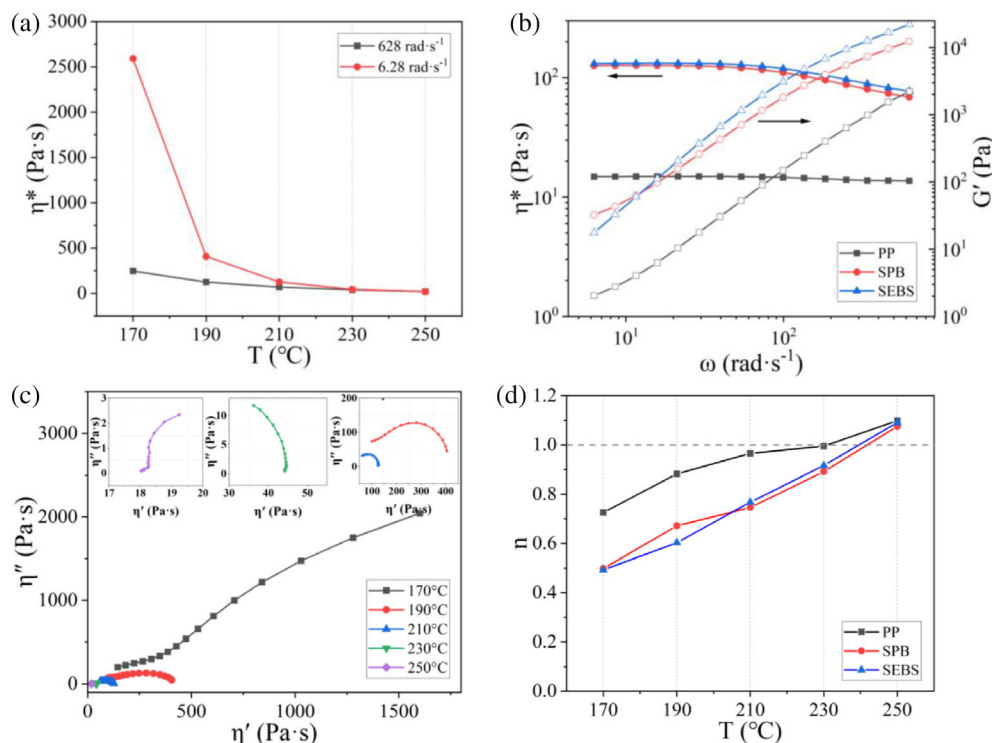


**FIGURE 3** The rheological properties of SEBS, PP and SPB: (a) complex viscosity ( $\eta^*$ ) of SPB vs. temperatures with angular frequency ( $\omega$ ) of 628  $\text{rad s}^{-1}$  and 6.28  $\text{rad s}^{-1}$ , (b) storage modulus ( $G'$ ) and complex viscosity ( $\eta^*$ ) vs. angular frequency ( $\omega$ ) at 210°C, (c) Cole-Cole curves of SPB at different temperatures, (d) non-Newtonian index ( $n$ ) under different temperatures [Color figure can be viewed at [wileyonlinelibrary.com](http://wileyonlinelibrary.com)]

deviated from a semicircular shape again, which may have been due to thermal degradation and crosslinking of the polymers causing phase separation.

The non-Newtonian index ( $n$ ) was calculated using Equation (6),<sup>41</sup>

$$\lg \eta_a = \lg K + (n - 1) \lg \dot{\gamma}, \quad (6)$$

where  $\eta_a$  is the apparent viscosity,  $K$  is the consistency,  $n$  is the non-Newtonian index and  $\dot{\gamma}$  is the shear frequency. As shown in Figure 3d, the  $n$  values of SEBS, SPB and PP increased with increases in temperature, indicating that the mobility of the polymers improved and tended toward the behavior of a Newtonian fluid. As the temperature approached 250°C, the viscosity in the high angular frequency region increased and the  $n$  values were larger than unity. This may be assigned to a dilatant (shear thickening) flow caused by high orientation of the molecular chains along the shear direction.

In summary, the SPB exhibited an excellent, steady melt flow at temperatures between 210 and 230°C. These temperatures were chosen for polymer extruding during melt blowing.

### 3.4 | Morphology and fiber diameter distribution of SPB nonwovens

Elastic nonwovens were prepared by using SPB in a melt-blowing process. The typical surface and cross-

section morphology are shown in Figure 4. The random orientation and course entanglement between fibers, which is a typical structure of melt blown nonwovens, arose from the thermal self-bonding and stickiness of polymers. The cross-section morphology of fibers is shown in Figure 4g, which exhibited a typical sea-island structure, in which PP dispersed in the SEBS matrix as an island phase. As the Cole-Cole plots revealed, this phenomenon demonstrated that, although PP and SEBS to some extent, had a compatibility at the process temperature, phase separation occurred during the formation of fibers.

It also can be seen from Figure 4a–f that there were fiber strands appeared in the nonwovens which were caused by insufficient solidification of the fibers when they reached the collector. With increasing air pressure and decreasing DCD, the number of fiber strands increased (as circled in red in the images). This can be attributed to the shorter time for fibers to be drawn and cooled at shorter DCD and higher air pressure, resulting in lower fiber solidification and higher temperature. Fiber bundles were more likely to form when fibers were in contact with other fibers on the collector.

The heightened fiber intensity also illustrated that too high an air pressure or too short a DCD would lead to rough surfaces and fiber strands, influencing the appearance of nonwovens.

The fiber diameters under different air pressures and DCDs are shown in Figure 4h, i. The mean fiber diameter decreased from 13.70 to 11.91  $\mu\text{m}$  as the air pressure



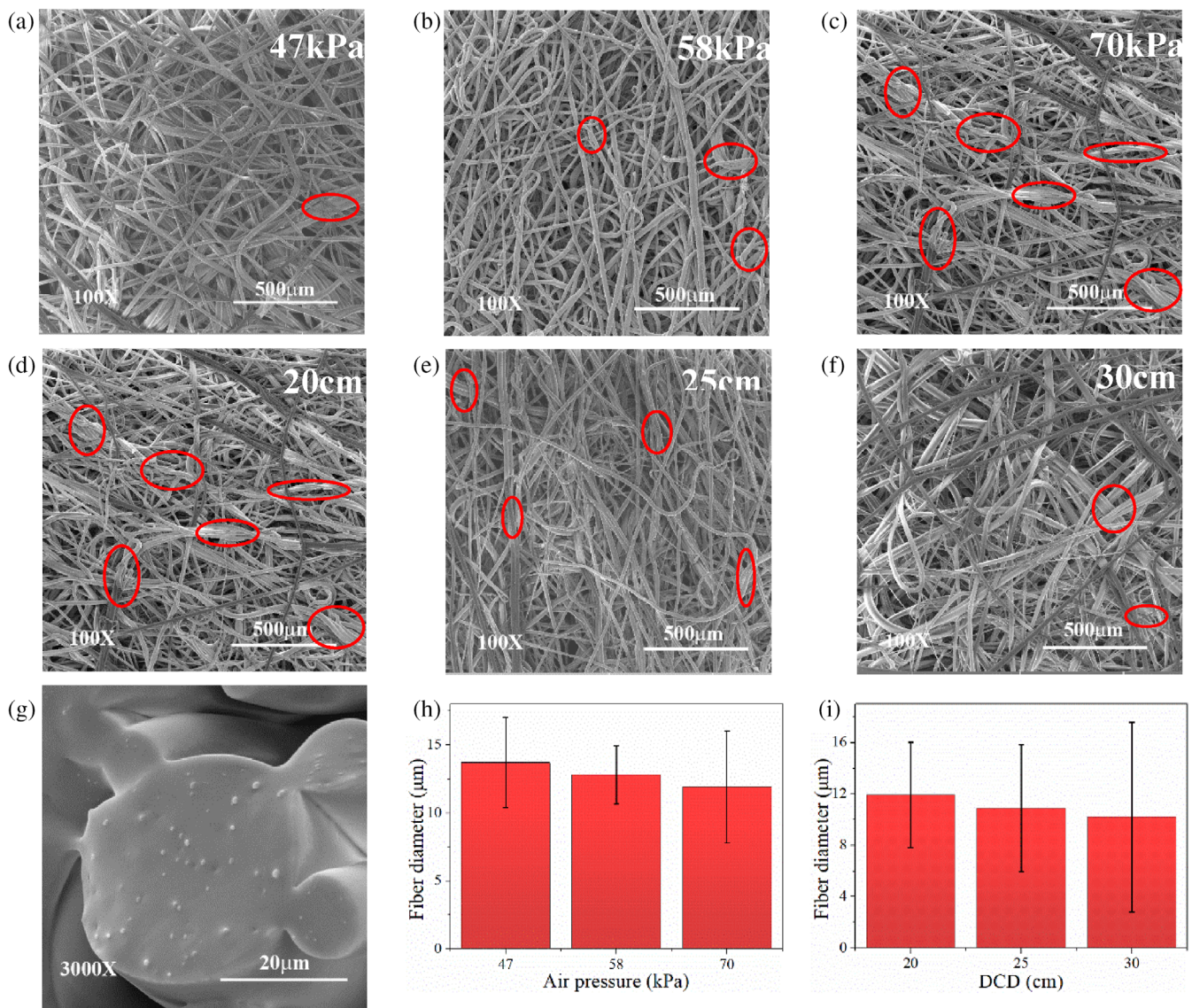


**FIGURE 4** The fiber distribution and bonding configurations of SPB nonwovens: (a)–(c) under different air pressures at DCD 20 cm, (b)–(d) under different DCDs at an air pressure 70 kPa (fiber strands are circled in red in images), (g) cross-section image of fibers, (h) and (i) the fiber diameter distribution at a DCD of 20 cm and an air pressure 70 kPa [Color figure can be viewed at [wileyonlinelibrary.com](https://onlinelibrary.wiley.com/terms-and-conditions)]

increased from 47 to 70 kPa. With the increase in air pressure, the stretch velocity before the fiber reached the web collector increased, the fibers became thinner and the dispersion of diameters increased. The same trend was observed when the DCD increased from 20 to 30 cm with the fiber diameter decreasing from 20 to 30 cm with the fiber diameter decreasing from 11.91 to 10.19  $\mu\text{m}$ . With the distance from die to collector increased, the time for fiber attenuation and fibrillation increased so that the fiber diameter decreased accordingly and thinner fibers were formed. Both the increase in air pressure and DCD resulted in a decrease in fiber diameter, and the effect of DCD was more pronounced. Further increases in DCD and air pressure are expected to produce finer fibers.

### 3.5 | Effects of air pressure and DCD on the porosity of SPB nonwovens

Melt blown nonwoven are porous mats, high porosity provides breathability and barrier properties during application. The porosity reflects the ratio of the pore of a nonwoven mat, which is related to fiber fineness and bonding situation, and these characteristics are influenced by process parameters. As shown in Figure 5, porosity decreased when air pressure increased, and increased as DCD increased.

The high air pressures provided high velocities when fibers broke loose from the die. Finer fibers would be obtained under the higher stretch rates and they collapse

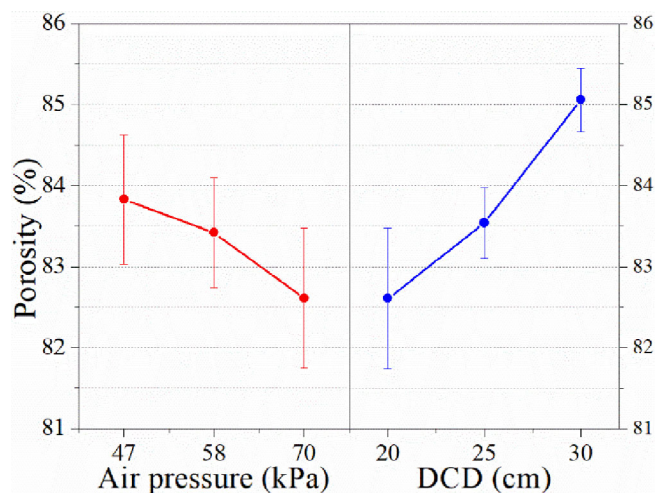


**FIGURE 5** The effects of air pressure and DCD on the porosity of SPB nonwovens [Color figure can be viewed at [wileyonlinelibrary.com](https://onlinelibrary.wiley.com/doi/10.1002/app.53308)]

more easily into denser structures.<sup>12</sup> Besides, the higher velocities leading to shorter times for fibers to reach the collector, the insufficient cooling and solidification would enhance the self-bonding of fibers to form denser nonwoven mats with lower porosity.

The effects of DCD on porosity were complex. On one hand, the high DCD would lead to thinner fibers, forming denser structures. On the other hand, higher DCD also meant longer distances and longer times for fibers to be suspended in air. Also, more cooling and solidification took place before fibers reached the collector. This would reduce the self-bonding ability among fibers and form fluffier nonwoven mats with higher porosity. The results showed that the effect of the bonding is more critical than that of the fiber diameter in this work.

The influences of air pressure and DCD on porosity were opposite, and the variation of porosity with DCD was more obvious. However, the porosity of the samples obtained in this work was between 80% and 90%, which is consistent with the porosity of PP melt blown nonwoven fabrics (75%–95%),<sup>8</sup> reflecting that the SPB nonwoven can be used in the fields that with high porosity requirements.

### 3.6 | Effects of air pressure and DCD on tensile properties of SPB nonwovens

Mechanical properties play a significant role in the application of nonwovens. There are many factors that can affect these mechanical properties, including the properties of the fibers, the bonding situation and the alignment of fibers. The typical stress–strain curves of

SPB nonwovens are shown in Figure 6a, b, the tensile strength and elongation at peak under different air pressures and DCDs are presented in Figure 6c, d. It can be seen that the tensile strength in the machine direction (MD) increased with air pressure increases and decreased with increasing DCD, while for the tensile strength in the cross direction (CD) and elongation in both MD and CD, the trends were more complex.

With air pressure increases, the stretching force on fibers along the MD increased, and the crystallinity and orientation of the PP in the SPB blend was enhanced, thereby improving tensile properties. Meanwhile, the solidification of the fibers decreased with the increase of air pressure, leading to increase of the bonding strength between fibers which were conducive to enhance the tensile strength and elongation of nonwovens. In MD, the tensile strength and elongation of fibers increased with the increase of the air pressure because of the increased crystallinity and bonding strength. In CD, due to the number of fibers arranged in this direction decreased with the increase of the air pressure, the bonding points of the fibers in the CD decreased, which hindered the increase of tensile strength and elongation of nonwovens. Therefore, the tensile strength and elongation in CD initially decreased and then increased.

When the DCD increased from 20 to 30 cm, PP molecules had more time to form higher crystallinity and enhanced orientation, which was beneficial to the improvement of the strength of the nonwovens, but the bonding strength among fibers declined due to the cooling and solidification before reaching the collector, which will reduce the strength and elongation of the nonwovens. The fiber alignment was more random leading to the number of bonding points in MD decreasing and those in CD increasing. In MD, the number of fiber bonding points decreased, along with the decrease in fiber bond strength, resulting in the decrease in tensile strength and elongation with increasing DCD. In CD, although the increase in the number of fibers and bonding points was beneficial to the increase in strength, the tensile strength of the nonwoven fabric still decreased under the influence of the decrease in the fiber bonding strength but the decrease is smaller than that in MD. Furthermore, the elongation of fibers in CD increased before decreasing.

### 3.7 | Effects of air pressure and DCD on elastic recovery of SPB nonwovens

Elastic recovery properties are important for materials used in flexible products. The strain recovery ratio under 100% elongation is used to assess elastic recovery

**FIGURE 6** The typical stress–strain curves of SPB nonwovens, (a) under different air pressures at DCD 20 cm, (b) under different DCDs at an air pressure 70 kPa, (c) and (d) the effects of air pressure and DCD on the tensile properties of SPB nonwovens [Color figure can be viewed at [wileyonlinelibrary.com](https://onlinelibrary.wiley.com/doi/10.1002/app.53308)]

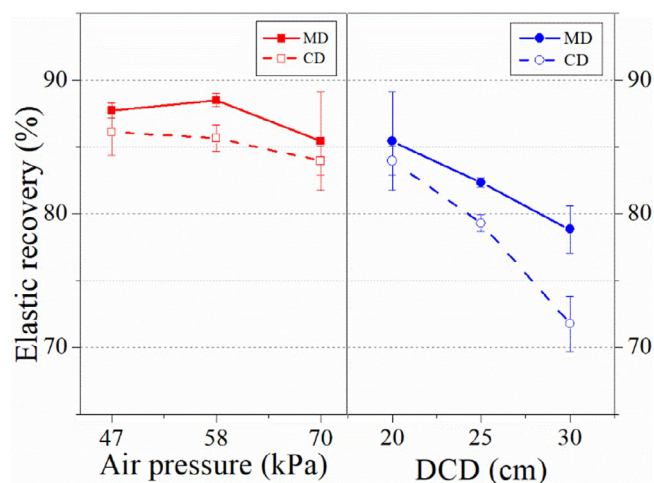
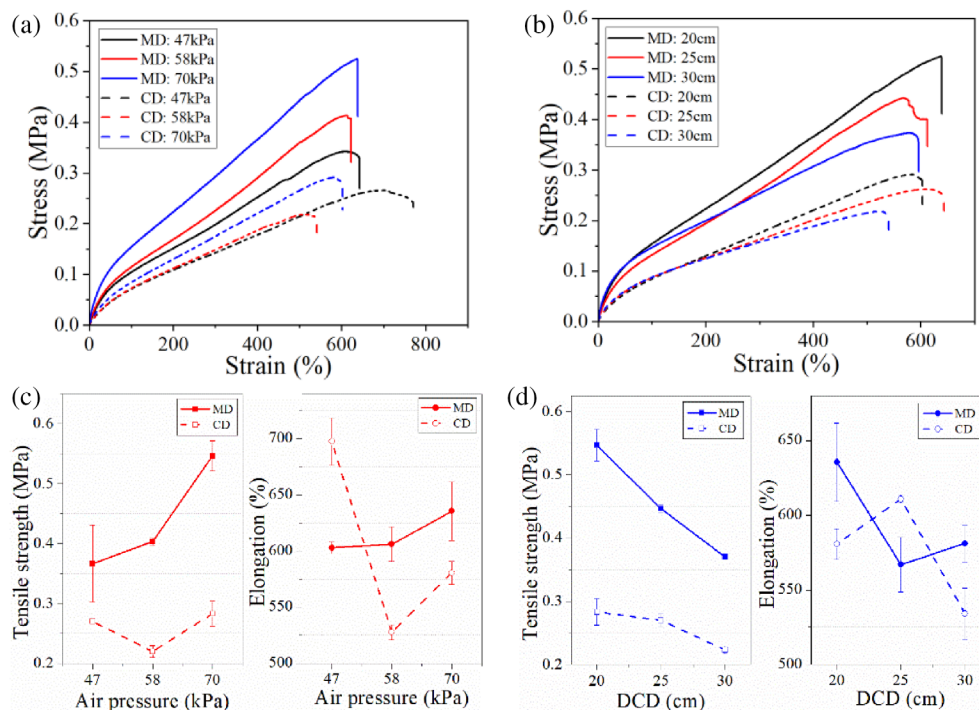


**FIGURE 7** The effects of air pressure and DCD on the elastic recovery properties of SPB nonwovens [Color figure can be viewed at [wileyonlinelibrary.com](https://onlinelibrary.wiley.com/doi/10.1002/app.53308)]

behavior. For the nonwovens, the variation of elastic recovery is mainly influenced by the inherent elastic properties of SEBS and the structure of nonwovens, especially the bonding strength. It can be seen from Figure 7 that the elastic recovery rate decreases with the increase of air pressure and DCD, but it varies slightly with increasing air pressure increases, and declines significantly with increasing DCD.

With air pressure increases, although the fiber bonding strength increased, benefiting elastic recovery, the limitation of PP chains to EB segments increased with enhanced crystallinity and orientation of the PP, which

reduced the ability of the SEBS to recover. Due to these, the elastic recovery rate of the nonwoven fabric decreased slightly with the increase of air pressure.

With DCD increases, the higher crystallinity and orientation of the PP molecules restricted the elongation and recovery of the EB molecular chains more significantly. Simultaneously, the bonding strength between fibers became weaker with thinner fibers and higher porosity. When an external force was applied, the deformation of a nonwoven structure proved difficult to recover, resulting in a more pronounced decrease in elastic recovery.

## 4 | CONCLUSION

The structure of SPB phase separation was explored by investigating morphology and rheological properties of SPB. The results showed that in the range of 210–230°C, the molten blend was compatible and stable with a flow index approaching 0.9. This provided an optimized polymer extrusion temperature for the subsequent melt blowing process. The crystallizing behavior of SPB was also studied. In the blend, the crystalline structure of PP was rarely changed but slower crystallization and finer crystals occurred higher levels of undercooling.

Elastic nonwovens based on SPB were manufactured using the melt blowing process. The effects of air pressure and DCD on the morphology structure and properties of nonwovens were discussed. The results revealed that with increases in air pressure, the fiber diameters decreased and the bonding strength among fibers was enhanced. As

a result, the porosity of nonwovens decreased and tensile strength increased with a slight decrease in elastic recovery rates. Finer fibers and weaker bonding strength resulted from increasing DCD leading to higher porosity, lower tensile strength and elastic recovery.

### AUTHOR CONTRIBUTIONS

**Li Chang:** Data curation (lead); investigation (lead); writing – original draft (lead). **Yanfen Zhou:** Methodology (equal); writing – review and editing (equal). **Kun Dai:** Visualization (lead). **Liang Jiang:** Methodology (equal); supervision (equal); validation (equal); writing – review and editing (equal). **Stephen Jerrams:** Writing – review and editing (equal). **Jianwei Ma:** Supervision (equal); validation (equal). **Shaojuan Chen:** Funding acquisition (lead); project administration (lead).

### ACKNOWLEDGMENT

The authors would like to acknowledge the financial assistance provided by the Key R & D project of Shandong Province (No 2018GGX108003).

### DATA AVAILABILITY STATEMENT

Research data are not shared.

### ORCID

Liang Jiang  <https://orcid.org/0000-0002-7792-6069>

### REFERENCES

- [1] N. Karim, S. Afroj, K. Lloyd, L. C. Oaten, D. V. Andreeva, C. Carr, A. D. Farmery, I. D. Kim, K. S. Novoselov, *ACS Nano* **2020**, *14*, 12313.
- [2] H. Saleem, L. Trabzon, A. Kilic, S. J. Zaidi, *Desalination* **2020**, *478*, 14178.
- [3] A. Alassod, M. A. Abedalwafa, G. Xu, *Environ. Technol.* **2021**, *42*, 2784.
- [4] V. A. Wente, *Ind. Eng. Chem.* **1956**, *48*, 1342.
- [5] R. K. Campos, J. Jin, G. H. Rafael, M. Zhao, L. Liao, G. Simmons, S. Chu, S. C. Weaver, W. Chiu, Y. Cui, *ACS Nano* **2020**, *14*, 14017.
- [6] X. Y. D. Soo, S. Wang, C. C. J. Yeo, J. Li, X. P. Ni, L. Jiang, K. Xue, Z. Li, X. Fei, Q. Zhu, X. J. Loh, *Sci. Total Environ.* **2022**, *807*, 151084.
- [7] Y. Gu, B. Wang, Z. Dong, Q. Zhang, J. Wu, X. Zhang, *New Chem. Mater.* **2021**, *49*, 214.
- [8] K. C. Dutton, *J. Textile Apparel Technol. Manag.* **2009**, *6*, 1.
- [9] J. A. Austin, EP1443132, **2004**.
- [10] G. He, L. Wang, X. Bao, Z. Lei, F. Ning, M. Li, X. Zhang, L. Qu, *Composites, Part B* **2022**, *232*, 109618.
- [11] T. Zapletalova, S. Michielsen, B. Pourdeyhimi, *J. Eng. Fiber Fabr.* **2006**, *1*, 62.
- [12] Y. E. Lee, PhD, University of Tennessee, USA, **2004**.
- [13] Y. Yu, E. Shim, *J. Appl. Polym. Sci.* **2020**, *138*, e50230.
- [14] D. L. Safranski, J. M. Boothby, C. N. Kelly, K. Beatty, N. Lakhera, C. P. Frick, A. Lin, R. E. Guldberg, J. C. Griffis, *J. Mech. Behav. Biomed. Mater.* **2016**, *62*, 545.
- [15] W. A. Duncan, US200912566564, **2018**.

- [16] Y. F. Zhou, L. Jiang, H. Y. Jia, X. L. Xing, Z. H. Sun, S. J. Chen, J. W. Ma, S. Jerrams, *Fiber. Polym.* **2019**, *20*, 1200.
- [17] M. N. Peng, H. Y. Jia, L. Jiang, Y. F. Zhou, J. W. Ma, *J. Text. I.* **2019**, *110*, 468.
- [18] T. J. Wisneski, M. T. Morman, US4663220, **1987**.
- [19] X. T. Shi, J. X. Wu, X. P. Zhen, H. S. Xie, C. Z. Xiong, *Polym. Adv. Technol.* **2019**, *30*, 2370.
- [20] F. O. M. S. Abreu, M. M. C. Forte, S. A. Liberman, *J. Appl. Polym. Sci.* **2005**, *95*, 254.
- [21] Z. Liu, C. Li, X. Zhang, B. Zhou, S. Wen, Y. Zhou, S. Chen, L. Jiang, S. Jerrams, F. Zhou, *ACS Sustainable Chem. Eng.* **2022**, *10*, 8788.
- [22] B. Zhou, C. Li, Y. Zhou, Z. Liu, X. Gao, X. Wang, L. Jiang, M. Tian, F.-L. Zhou, S. Jerrams, J. Yu, *Compos. Sci. Technol.* **2022**, *224*, 109478.
- [23] Flood, J. E, H. JR, D. L, EP2428534, **2012**.
- [24] S. Setz, F. Stricker, J. Kressler, T. Duschek, R. Mlhaupt, *J. Appl. Polym. Sci.* **1996**, *59*, 1117.
- [25] C. I. Ribeiro De Oliveira, M. C. Guimaraes Rocha, J. T. de Assis, A. L. Nazareth Da Silva, *J. Thermoplast. Compos. Mater.* **2022**, *35*, 281.
- [26] A. K. Gupta, K. R. Srinivasan, *J. Appl. Polym. Sci.* **1993**, *47*, 167.
- [27] A. Gupta, S. Purwar, *J. Appl. Polym. Sci.* **1985**, *30*, 1777.
- [28] G. Holden, E. T. Bishop, N. R. Legge, *J. Polym. Sci., Part C: Polym. Symp.* **1969**, *26*, 37.
- [29] L. Chang, C. Wu, P. Lan, B. Bai, L. Jiang, S. Chen, S. Jerrams, J. Ma, *Text. Res. J.* **2021**, *92*, 1620.
- [30] Q. A. Bresee, M. C. Pelham, *Int. Nonwovens J.* **2005**, *os-14*, 1558925005os.
- [31] Q. U. A. Bresee, *Int. Nonwovens J.* **2004**, 1558925004os. <https://doi.org/10.1177/1558925004os-1300113>.
- [32] G. Sun, J. Yang, S. Xin, R. Yu, X. Wang, *Ind. Eng. Chem. Res.* **2018**, *57*, 9707.
- [33] N. D. Yilmaz, P. Banks-Lee, N. B. Powell, S. Michielsen, *J. Appl. Polym. Sci.* **2011**, *121*, 3056.
- [34] L. E. Alexander, *X-ray Diffraction Methods in Polymer Science*, Wiley Interscience, New York **1969**.
- [35] H. J. Cai, X. L. Luo, X. X. Chen, D. Z. Ma, J. M. Wang, H. S. Tan, *J. Appl. Polym. Sci.* **1999**, *71*, 103.
- [36] R. R. Mocerlini, O. A. Lambri, C. L. Matteo, J. A. García, G. I. Zelada-Lambri, P. A. Sorichetti, F. Plazaola, A. Rodríguez-Garraza, F. A. Sánchez, *Polymer* **2009**, *50*, 4696.
- [37] F. G. Bonifacich, O. A. Lambri, F. D. Lambri, P. B. Bozzano, V. Recarte, V. Sánchez-Alarcos, J. I. Pérez-Landazábal, *Mech. Mater.* **2021**, *162*, 104045.
- [38] F. G. Bonifacich, O. A. Lambri, V. Recarte, V. Sánchez-Alarcos, J. I. Pérez-Landazábal, *Compos. Sci. Technol.* **2021**, *201*, 108538.
- [39] T. Ougizawa, S. A. Madbouly, T. Inoue, *Macromol. Symp.* **2000**, *149*, 69.
- [40] B. Afsari, M. K. Razavi Aghjeh, M. Hasanpour, *Rheol. Acta* **2020**, *59*, 399.
- [41] H. Eshgarf, M. Afrand, *Exp. Therm. Fluid Sci.* **2016**, *76*, 221.

**How to cite this article:** L. Chang, Y. Zhou, K. Dai, L. Jiang, S. Jerrams, J. Ma, S. Chen, *J. Appl. Polym. Sci.* **2023**, *140*(2), e53308. <https://doi.org/10.1002/app.53308>